CRYSTAL GROWTH & DESIGN

pubs.acs.org/crystal

Article

# Probing the Magnetization Relaxation Dynamics of Four-Coordinate Lanthanide(III) Complexes

*Published as part of a Crystal Growth and Design virtual special issue on Molecular Magnets and Switchable Magnetic Materials*

Dipanti Borah,[‖] Amaleswari Rasamsetty,[‖] Deepanshu Chauhan, Shalini Tripathi, Felix Houard, Olivier Cador, Kevin Bernot, Gopalan Rajaraman,* and Maheswaran Shanmugam*

Cite This: *Cryst. Growth Des.* 2023, 23, 629–636

Read Online

ACCESS | Metrics & More | Article Recommendations | Supporting Information

**ABSTRACT:** The reaction of bulky trimethylsilylanilide (N-TMSA) ligand with various lanthanide salts led us to isolate unusual and unique four-coordinate monomeric Ln(III) complexes which are challenging to isolate and not surprisingly rare in the literature. The single crystal X-ray diffraction unveils that all the complexes are monomeric and isostructural with the general molecular formula of $[Ln(N\text{-}TMSA)_3(THF)]$ where Ln = Dy (**1**) or Yb (**2**). Both complexes are found to possess distorted tetrahedral geometry. For all the complexes, detailed dc and ac susceptibility measurements were performed and both **1** and **2** show frequency-dependent out-of-phase susceptibility signals only in the presence of an optimum external magnetic field. The experimental observations are well supported by theoretical calculations and developed magneto-structural correlation using the various model complexes.

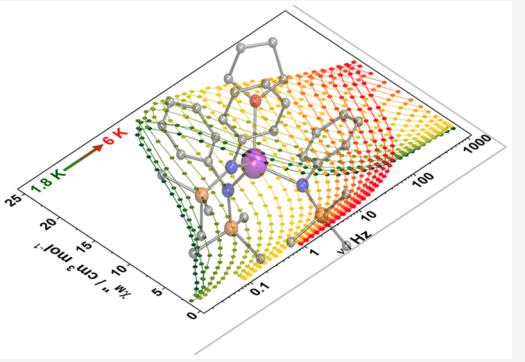


## INTRODUCTION

The presence of unquenched orbital angular momentum in lanthanide ions constitutes not only a large magnetic moment but also large magnetic anisotropy,[1−3] which makes them an attractive candidate for the development of new magnetic materials. Due to this reason, even a mononuclear Tb(III)−$Pc_2$ complex (Pc = phthalocyanine) is capable of showing a large effective energy barrier for the magnetization vector reversal reported by Ishikawa et al. in 2003.[4] Such types of complexes are termed single-ion magnets (SIMs). Following this discovery, lanthanide-based SIMs flooded the literature as they are envisaged to possess various potential applications such as in dense information storage devices,[5] spintronics,[6] qubits, qudits,[7−9] etc. Besides the detailed experimental work, *ab initio* calculations have highlighted the influence of the crystal field on the magnetic anisotropy axis orientations in various lanthanide ion complexes, i.e., the need to maximize the axial anisotropy of the lanthanide ion depending upon the shape of the f-electron density.[10] This was elegantly put forward by Long and co-workers in an amenable ligand field model to have strong magnetic anisotropy in various Ln(III) ions.[11]

Through the efforts of various researchers, it is now well understood that maintaining the proper ligand field around the Ln(III) ions is a way to enhance the effective energy barrier by reducing the quantum tunneling of magnetization and thereby enhancing the blocking temperature.[12] However, controlling the ligand field around the lanthanide ions is a challenging task due to their large ionic radius size that favors a large coordination number ranging from 7 to 12.[3,13,14]

So, reducing the coordination number around the lanthanides or maintaining a suitable crystal field based on the oblate or prolate f-electron density appears to be an excellent strategy to enhance the axial anisotropy.[15] Based on these design principles, several groundbreaking results have been achieved recently. For example, various cyclopentadienyl (Cp) derivatives of Dy(III) complexes enhance the blocking temperature ($T_B$) of the molecule close to liquid nitrogen temperature.[16,17] In a similar line, Nippe and co-workers have shown that a homoleptic borolide sandwich complex of Dy(III) was found to maintain better linearity that tends to increase the axiality which pushes the $T_B$ to 66 K.[18] The other class of Dy(III) complexes belongs to a pseudo linear complex where a strong axial ligand and weak equatorial ligand also maintain the strong axial anisotropy. For example, various pentagonal/hexagonal bipyramidal Dy(III) complexes were reported by Winpenny and co-workers, Murugavel and co-

**Received:** October 31, 2022
**Revised:** November 23, 2022
**Published:** December 19, 2022







https://doi.org/10.1021/acs.cgd.2c01246
*Cryst. Growth Des.* 2023, 23, 629−636

workers, Tong and co-workers, Murrie and co-workers, and others independently.[2,19−26]

The influence of crystal field on magnetization relaxation dynamics of numerous Ln(III) complexes with coordination numbers 7−12 is well studied in the literature.[3,13,14] On the contrary, lanthanide complexes with less than 7 coordination numbers are extremely few.[27−29] This is attributed to the synthetic challenge involved in stabilizing coordinatively unsaturated Ln(III) complexes. To isolate low coordinate Ln(III) complexes, predominantly bulky alkoxide or aryloxide ligands were employed.[30] Among the various coordination numbers, the lanthanide complexes with four coordination are extremely scarce in the literature. Only a handful of homoleptic and heteroleptic amide/alkoxide ligands were employed to isolate such systems, which are important for the development of the structure−property correlations.[31−35]

Therefore, we intend to isolate a series of four-coordinate Ln(III) complexes using the bulky trimethylsilylanilide (N-TMSA) ligands and study their electronic and magnetic properties. In this Article, we report two structurally analogous four-coordinate Ln(III) complexes with the general molecular formula of $[Ln(N\text{-}TMSA)_3(THF)]$ where Ln = Dy (**1**) or Yb (**2**), which are characterized by single crystal X-ray diffraction. For all the complexes, detailed dc and ac magnetic susceptibility measurements were performed. Both complexes **1** and **2** show frequency-dependent out-of-phase susceptibility signals only in the presence of an optimum external magnetic field. Further, their detailed electronic structure and the mechanism of their magnetic relaxation were investigated through *ab initio* calculations.

## EXPERIMENTAL METHODS

The details of the materials and additional methods are included in the Supporting Information.

**Synthesis of Complex $[Dy(N\text{-}TMSA)_3(THF)]$ (1).** In a Schlenk tube, one equivalent of anhydrous $DyCl_3$ (0.389 mmol, 0.105 g) and three equivalents of lithium trimethylsilylanilide (Li(N-TMSA)) (1.168 mmol, 0.2 g) were taken. These were dissolved in dry THF (10 mL), and the entire contents were stirred for 12 h at room temperature. After 12 h, the solvent was stripped off under reduced pressure. The product of interest was extracted from dry hexane (5 mL) and filtered. The filtrate was kept for crystallization at −27 °C. Pale pink colored, block-shaped crystals were grown from the filtrate after 1 day. The yield (based on $DyCl_3$) of **1**: 0.033 g (12%). Elemental analysis (Calcd %): C, 51.18; H, 6.93; N, 5.78; Found (%): C, 51.27; H, 7.12; N, 5.83.

**Synthesis of Complex $[Yb(N\text{-}TMSA)_3(THF)]$ (2).** A similar synthetic procedure as in **1** was followed to isolate **2**, but $YbCl_3$ (0.389 mmol, 0.109 g) was used in place of $DyCl_3$. Dark orange colored, block-shaped crystals were grown from the filtrate after 1 day. The yield (based on $YbCl_3$) of **2**: 0.038 g (13%). Elemental analysis (Calcd %): C, 50.45; H, 6.83; N, 5.69; Found (%): C, 50.12; H, 6.42; N, 5.11.

## RESULTS AND DISCUSSION

The reaction of anhydrous $LnCl_3$ in the presence of Li(N-TMSA) ligand in THF, followed by crystallization in hexane, led us to isolate single crystals which were suitable for single crystal X-ray diffraction (Scheme 1). The single crystal X-ray structure determination of all the complexes reveals the molecular formula as $[Ln(N\text{-}TMSA)_3(THF)]$ (where Ln = Dy (**1**) or Yb (**2**); Figure 1). The complexes were solved in the monoclinic, $P2_1/n$ space group. All the complexes are structurally analogous to each other which is also clearly reflected in the unit cell parameters of all the complexes (Table S1). We would like to point out that these complexes' single-crystal X-ray structures were reported by Evans and co-workers in 2019, but magnetic studies have not been performed on these complexes.[36]

**Scheme 1. General Synthetic Procedure Followed to Isolate Complexes 1 and 2**

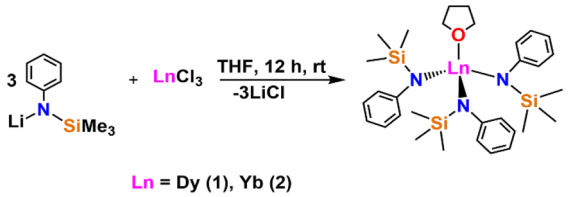


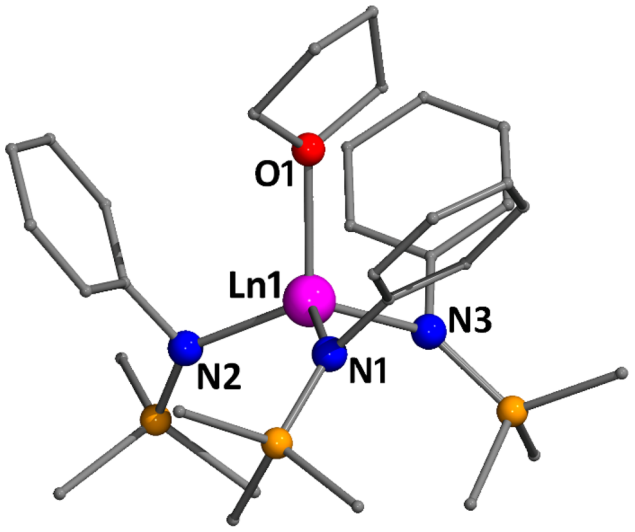


**Figure 1.** Ball and stick representation of the crystal structure of complexes **1** and **2** (where Ln = Dy (**1**) and Yb (**2**)). Color code: $Ln^{III}$ = magenta; O = red; N = blue; C = gray; Si = orange.

Therefore, the structural description of one of the representative complexes (complex **1**) is described below. The single crystal X-ray diffraction reveals that all the complexes are mononuclear and are surrounded by three anilide ligands. The fourth coordination is completed by a THF molecule, thus exhibiting distorted tetrahedral geometry. The observed geometry around the Ln(III) complexes was also confirmed by the Continuous Shape measurement (CShM) software (Table S2).[37] The average Dy−N and Dy−O bond distances were found to be 2.231(7) and 2.319(5) Å (see also Table 1 for the selected bond distances and bond angles for both the complexes). Due to the lanthanide contraction, the Ln−N or Ln−O distances decreased as we move along the group from Dy(III) to Yb(III).[38]

As the size of the Ln(III) ions are larger than 3d metal ions, they usually prefer a larger coordination number (in the range of 7−12). However, the isolation of lanthanide complexes with a coordination number less than 7 is always an uphill process. Considering this aspect, the isolated four-coordinate Ln(III) complexes are synthetically challenging and unique. Consequently, the literature reports on such unusual geometry and their magnetic properties are extremely scarce. Coordination chemistry of anilide ligands is well established to isolate coordinatively unsaturated transition metal complexes, on the other hand, and such chemistry is extremely rare in lanthanides due to their oxophilicity.


https://doi.org/10.1021/acs.cgd.2c01246
Cryst. Growth Des. 2023, 23, 629−636

Table 1. Selected Bond Lengths and Bond Angles of 1 and 2

| | 1 | 2 |
|---|---|---|
| | Bond Length/Å | |
| Ln1−O1 | 2.3197(5) | 2.2603(5) |
| Ln1−N2 | 2.2195(7) | 2.1746(8) |
| Ln1−N1 | 2.2428(7) | 2.1976(8) |
| Ln1−N3 | 2.2405(7) | 2.1926(8) |
| | Bond Angles/° | |
| N2−Ln1−O1 | 114.40(6) | 112.62(6) |
| N2−Ln1−N1 | 114.39(6) | 113.89(7) |
| N2−Ln1−N3 | 110.00(6) | 111.63(7) |
| N1−Ln1−O1 | 97.42(6) | 96.88(6) |
| N3−Ln1−O1 | 109.99(6) | 109.01(6) |
| N3−Ln1−N1 | 110.05(6) | 111.87(7) |

To better understand the supramolecular interactions within the crystal lattice of **1**, we have analyzed the packing diagram of the complex (Figure 2a). In **1**, we did not find any classical H-bonding or other supramolecular interactions. The shortest Dy···Dy distance is observed to be 9.621(6) Å. This suggests that the intermolecular interactions between the molecules in these complexes are expected to be extremely weak or nil. To quantify the various noncovalent interactions that stabilize the crystal lattice firmly, we have further performed Hirshfeld Surface (HS) analysis. One of the properties of the HS is $d_{norm}$ which is a symmetric function of the distances to the surface between nuclei inside ($d_i$) and outside ($d_e$) the HS, relative to their respective van der Waals radii. The various color-coded regions in the Hirshfeld surface indicates the various strength of the intermolecular interactions. The red and blue regions on the surface indicate the shorter and longer intermolecular contact, respectively, while that of white denotes the contact around the van der Waals radii. The HS of the complex (**1**; and also complex **2**) evidently shows that blue and white regions are predominant, implying that the intermolecular interactions are extremely weak (Figure 2b−d).

The careful analysis of the 2D fingerprint diagram of **1** discloses that the intermolecular H···H (92%) contacts are dominant compared to other intermolecular contacts such as H···C (3%). Therefore, the Hirshfeld analysis also supports the fact that extremely weak intermolecular interactions are present in these complexes **1** and **2**, and hence, their influence on the magnetization relaxation dynamics is expected to be weak or nil.

**Direct Current Magnetic Susceptibility Measurements of Complexes 1 and 2.** Temperature-dependent magnetic susceptibility measurements of the polycrystalline sample of both the complexes were performed in the temperature range of 300 to 2.0 K in the presence of an external magnetic field (1 kOe; Figure 3). The room temperature $\chi_M T$ values of 14.52 and 2.33 cm$^3$ K mol$^{-1}$ were observed for complexes **1** and **2**, respectively. These values are quite consistent with the theoretically expected $\chi_M T$ values of 14.17 and 2.57 cm$^3$ K mol$^{-1}$ for a magnetically independent ion. Upon decreasing the temperature, the $\chi_M T$ value of complexes **1** and **2** gradually decreases up to 100 K before it falls rapidly below this temperature and reaches a final value of 10.2 and 1.2 cm$^3$ K mol$^{-1}$ at 2.0 K. This $\chi_M T$ profile at the higher temperature of these complexes suggest that the depopulations of Stark levels and the low-temperature drop is attributed to the inherent magnetic anisotropy associated with the complexes. Field-dependent magnetization measurements were performed for both complexes up to 50 kOe at 2.0 K. In all complexes, magnetization values increase with the magnetic field and magnetization values tend to saturate around 4.9 and 2.0 N$\mu_B$ for complexes **1** and **2**. These values are in agreement with the theoretically expected values from powder measurement of anisotropic samples **1** and **2**.

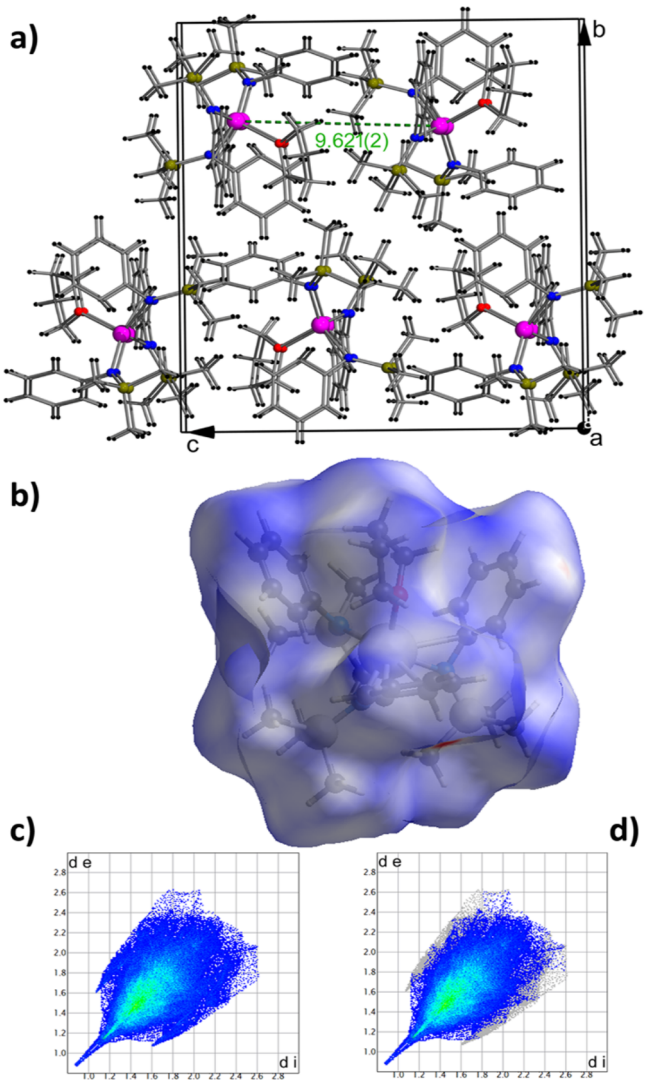


**Figure 2.** (a) The packing diagram of complex **1** along the *a*-axis. (b) Hirshfeld surface analysis mapped with $d_{norm}$ for **1**. (c, d) Two-dimensional (2D) fingerprint plots are shown for **1** (panel c for all intermolecular contact (100%) and panel d for H···H (92%) intermolecular contact) where di is the distance from the Hirshfeld surface to the nearest atom inside the surface and de is the distance from the nearest atom outside the surface.

**Alternating Current (ac) Relaxation Dynamics.** The magnetic relaxation dynamics were measured for the anisotropic complexes **1** and **2** with an oscillating magnetic field of 3 Oe in the frequency range of 0.02 to 1000 Hz in the temperature range of 1.8−6 K. Both complexes **1** and **2** did not show slow relaxation of magnetization in the absence of an external magnetic field. This implies that the crystal field around Dy(III) and Yb(III) promotes an underbarrier relaxation mechanism more efficiently than the thermally activated relaxation mechanism. To quench this fast quantum tunneling of magnetization (QTM), we have performed field-dependent ac-relaxation measurements. Through this study, we


https://doi.org/10.1021/acs.cgd.2c01246
Cryst. Growth Des. 2023, 23, 629−636

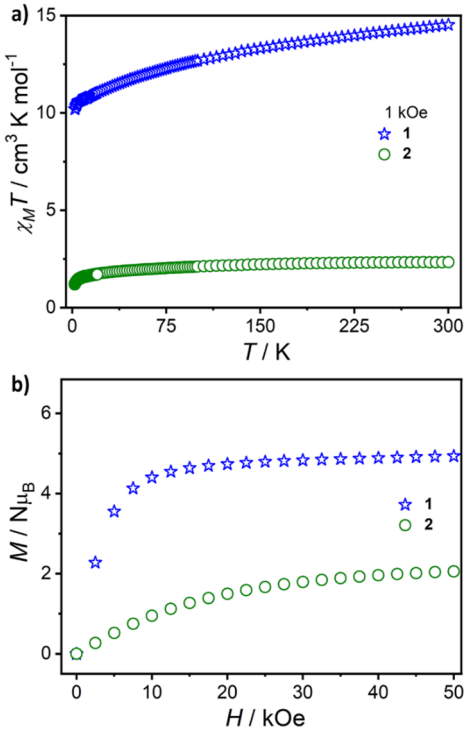


**Figure 3.** (a) Variable temperature dc magnetic susceptibility measurements performed on the polycrystalline samples of **1** and **2** in the presence of an external magnetic field of 1 kOe. (b) Isothermal (2 K) field-dependent magnetization measurements on complexes **1** and **2**.

have identified the optimum external magnetic field (a surprisingly low 0.4 kOe field for **1** and 1.2 kOe for **2**) where the relaxation is found to be slow for these complexes (Figures S1−S3). The ac susceptibility measured on polycrystalline samples **1** and **2** in the presence of an optimum external field indeed shows frequency-dependent out-of-phase susceptibility signals in the measured temperature range (Figure 4). This indicates that these two complexes possess field-induced slow relaxation of magnetization.

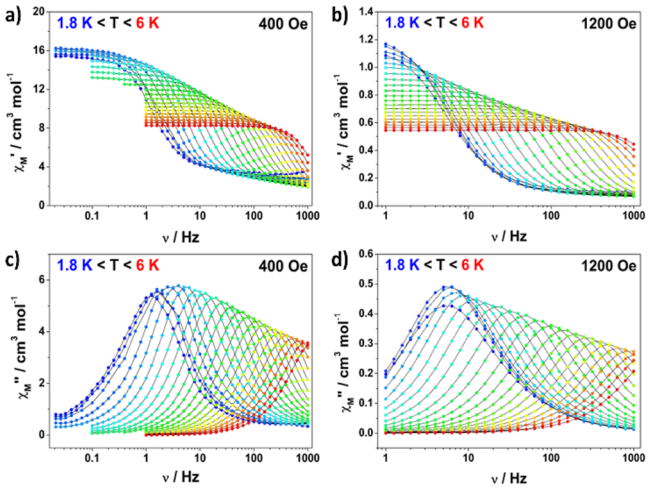


**Figure 4.** Frequency-dependent in-phase (panels a and b) and the out-of-phase signals (panels c and d) of **1** and **2** at the indicated dc external field in the temperature range of 1.8−6 K.

The Cole−Cole plot constructed from these data clearly emphasizes that only one type of relaxation is found in these complexes (Figure 5). The data were fitted using the

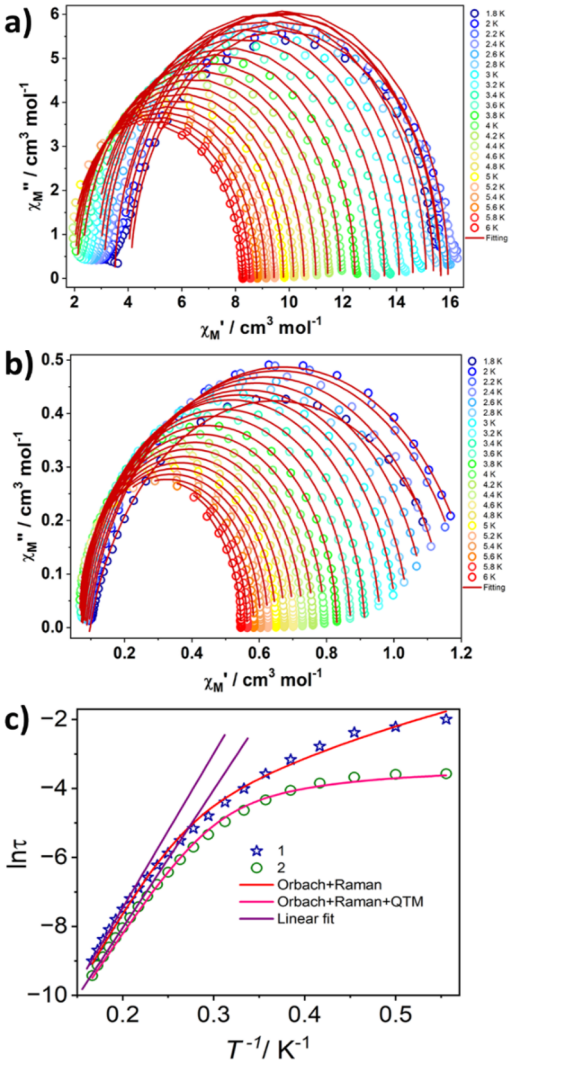


**Figure 5.** Cole−Cole plot of polycrystalline (a) sample **1** and (b) sample **2** in the presence of an external magnetic field. (c) Arrhenius plot of **1** and **2**.

generalized Debye model, and the extracted parameters are listed in Tables S3 and S4. The relaxation time extracted from the Cole−Cole data was employed to construct the Arrhenius plot. A linear trend is observed at the higher temperature regime while it deviates at lower temperatures. This indicates that, even at the optimum magnetic field, other faster relaxation processes such as Raman and/or Direct and/or QTM exist besides the Orbach process. The equation (eq 1) employed for fitting the Arrhenius plot is shown below:

$$\tau^{-1} = \tau_0^{-1} \times \exp(-U_{\text{eff}}/k_B T) + CT^n + \tau_{\text{QTM}}^{-1} \quad (1)$$

In the above equation, the three terms on the right-hand side indicate the Orbach, Raman, and QTM processes. For complex **1**, the QTM process is not necessary to fit the data, while for **2** all three processes were employed. The various parameters extracted upon fitting are shown in Table 2. The effective energy barrier for the magnetization reorientation is estimated


https://doi.org/10.1021/acs.cgd.2c01246
Cryst. Growth Des. 2023, 23, 629−636

Table 2. Best-Fit Parameters Obtained for the Arrhenius Plot of Complexes 1 and 2

| complexes | $U_{eff}/k_B$ (K) | $\tau_0$ (s) | $C$ ($s^{-1}\cdot K^{-n}$) | $n$ | $\tau_{QTM}$ (s) |
|---|---|---|---|---|---|
| 1 | 46.6 ± 1.7 | (5.35 ± 1.87) × $10^{-8}$ | 0.505 ± 0.09 | 4.15 ± 0.17 | |
| 2 | 40.0 ± 1.0 | (1.08 ± 0.21) × $10^{-7}$ | 0.695 ± 0.333 | 3.81 ± 0.43 | 0.032 ± 0.002 |

to be 46.6 and 40.0 K for **1** and **2**, respectively. The barrier height observed for **1** is slightly higher than the other four coordinate Dy(III) complexes reported in the literature,[31,34] while it is significantly lower than the barrier height of the $DyO_2Cl_2$ complex ($U_{eff}$ = 900 K) reported by Winpenny and co-workers.[32]

On the other hand, complex **2** is the first four-coordinate Yb(III) complex investigated for magnetization relaxation dynamics. The magnetization relaxation dynamics of four-coordinate lanthanide complexes are extremely rare. In this respect, the present work sheds light on the influence of this crystal field on the magnetization relaxation dynamics. Further, to better understand the electronic structure of these complexes and their relaxation mechanism, we have performed the *ab initio* calculations.

## THEORETICAL CALCULATIONS

To shed light on the mechanism of relaxation and the electronic structure of complexes **1** and **2**, we have performed *ab initio* CASSCF/RASSI-SO/SINGLE_ANISO calculations on the X-ray structures determined (Figure 6). The

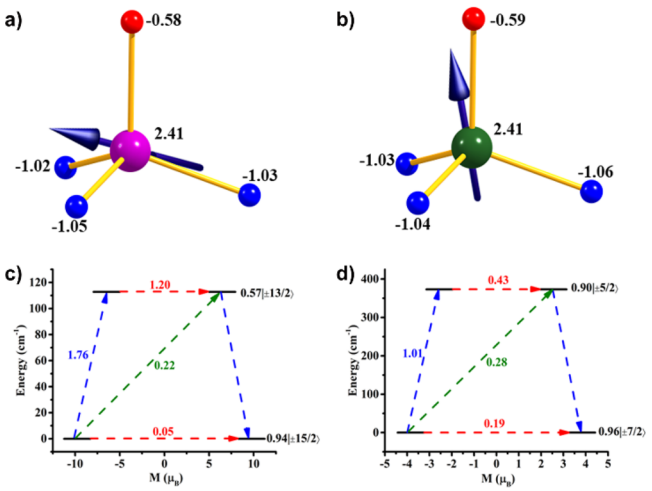


**Figure 6.** (a, b) Orientation of the magnetic anisotropy axis ($g_{zz}$). The numbers on the figures indicate the LoProp charge densities on the atoms of **1** and **2**, respectively. (c, d) The plausible relaxation mechanisms of **1** and **2**, respectively. In these panels, the red arrows show the QTM and TA-QTM via ground and first excited KDs. The green arrows show the Orbach process for relaxation. The blue arrows show the possible mechanism of magnetic relaxation. The black characters imply the $m_J$ composition of the KDs. Color code: Dy = magenta, Yb = green, O = red, and N = blue, other atoms omitted for clarity.

calculations reveal that the ground Kramers doublet (KD) of both the complexes possess axiality ($g_{zz}$ = 19.5, $g_{yy}$ = 0.2, $g_{xx}$ = 0.1 (for **1**) and $g_{zz}$ = 7.6, $g_{yy}$ = 0.6, $g_{xx}$ = 0.5 (for **2**)) and lacks Ising signature (Table 3). The presence of axiality in both these complexes is evidently reflected in the crystal field parameters computed. The crystal field parameter has been computed using the Stevens formalism

Table 3. Energies of Selected Computed KDs of 1 and 2

| | $g_x$ | $g_y$ | $g_z$ |
|---|---|---|---|
| | Complex **1** | | |
| KD1 | 0.105 | 0.221 | 19.529 |
| KD2 | 1.975 | 5.217 | 13.041 |
| | Complex **2** | | |
| KD1 | 0.505 | 0.652 | 7.673 |
| KD2 | 0.561 | 1.923 | 5.147 |

$\hat{H}_{CF} = \sum_{k=2,4,6} \sum_{q=-k}^{q=+k} B_k^q \hat{O}_k^q$ where $\hat{O}_k^q$ is the extended Stevens operator and $B_k^q$ is the crystal field parameter.[39] The comparable values of axial $B_k^q$ ($k$ = 0, $q$ = 0) and nonaxial $B_k^q$ ($k \neq 0$, $q$ = 2, 4) parameters imply significant QTM which is reflected in the relaxation mechanism (see Figure S4 and Tables S5 and S6). The computed nonzero and non-negligible rhombic $g$-tensors are well corroborated with this observation. Therefore, these two complexes are not expected to show magnetization blockade in the absence of an external magnetic field. This is consistent with the experimental observation where both **1** and **2** do not show frequency-dependent out-of-phase susceptibility signals in the absence of a dc-bias field.

The magnetization easy axis ($g_{zz}$) of the ground state KD of **1** and **2** lies along either Dy−N or Dy−O bond, respectively, with a tilt angle of 80° and 14.8°. The $g_{zz}$ axis for **1** and **2** are tilted from each other by ∼70°, suggesting a difference between the ground oblate density in **1** and prolate density in **2**. The eight KDs generated from the $^6H_{15/2}$ span up to 650.5 $cm^{-1}$ in **1**, and the four KDs generated from the $^2F_{7/2}$ state span up to 698.4 $cm^{-1}$ in **2** (Tables S7 and S8). Between complexes **1** and **2**, complex **1** was found to have a lesser QTM probability compared to **2** by an order of ∼3.8 times. This is essentially due to the unfavorable crystal field around certain lanthanide ions. However, if a suitable field is applied, the QTM at the ground state can be quenched, leading to relaxation via the first excited state. Experimentally, both the complexes do not exhibit zero-field SMM characteristics and required 0.4 and 1.2 kOe for **1** and **2**, respectively, to quench the ground state QTM effects. A three times larger magnetic field employed for **2** compared to **1** supports the computed QTM probability. The strong transverse anisotropy in the first excited KD leads to a large TA-QTM, which is coupled with a significant deviation of $g_{zz}$ from the ground KD and reinforces the magnetization vector relaxing back to the ground state via the first excited KD in both complexes. Therefore, the computed energy barrier for **1** and **2** is estimated to be 112.7 and 373.2 $cm^{-1}$, respectively (Figure 6). Achieving this theoretical estimate through the experimental measurement is unlikely as the ground state QTM probabilities are significant. This prediction is consistent with the experimental observation that both complexes are showing significantly low effective energy barriers (46.6 and 40 K for **1** and **2**, respectively) for the magnetization reversal (Figure 5c). The LoProp charges computed reveal the nitrogen atom in the equatorial ligand field has charges which are twice as much as those of the oxygen atom that lies along the pseudo $C_3$ axis direction (Figure 6a,b).[40]


https://doi.org/10.1021/acs.cgd.2c01246
Cryst. Growth Des. 2023, 23, 629−636

To further understand the role of axial ligand on the magnetization relaxation dynamics of **1** and **2**, we have performed calculations on the three coordinate model complexes where the THF ligands were removed in both Dy(III) and Yb(III) while leaving the other crystallographic parameters unchanged. These model complexes are called **1a** and **2a**, respectively (Tables S9−S36 and Figures S5−S32), hereafter. In these models **1a** and **2a**, to assess and analyze the nature of the pyramidalization angle, we have noted the deviation of the Ln(III) ion from the plane of the three nitrogen atoms as shown in Figure 7, inset by the parameter $\tau$

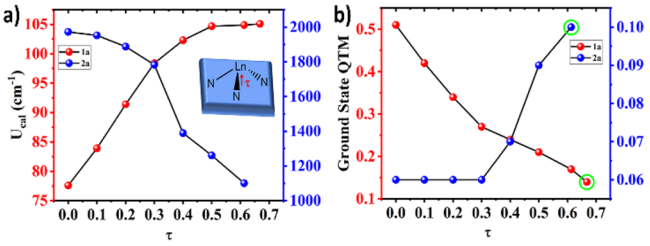


**Figure 7.** Magneto-structural correlation was performed to observe the effect of the out-of-plane-shift ($\tau$ parameter) on the computed $U_{cal}$ value.

(Å). As shown earlier by us, when $\tau$ = 0, a pseudo $D_{3h}$ condition is achieved and strong equatorial ligation is expected.[41] The $\tau$ value was found to be 0.668 and 0.613 Å for complexes **1a** and **2a**, respectively. We have noticed that, when $\tau$ = 0, the ground state KD QTM was substantially reduced in **2a** but increased in **1a** drastically. In **2a**, the QTM probability remains unchanged for the $\tau$ value in the range of 0−0.3 Å. A further increase of this leads to opening up the QTM within the ground KD, suggesting its tolerance level (Figure 7b), while a reverse trend was observed for **1a** (compared to **2a**); i.e., the highest QTM was observed when $\tau$ = 0, and then, it gradually decreases as the $\tau$ value increased. In line with QTM probability observed as a function of $\tau$-value for both models, the computed energy barrier ($U_{cal}$) values follow a similar trend for both **1a** and **2a** (Figure 7a).

To improvise the magnetic properties for Dy(III), it is clear that we need a stronger axial ligand and a larger $\tau$ value.

Besides these model calculations, we have generated another set of *in silico* models for **1** and **2**, where the axial THF was replaced by −F, −Cl, −Br, and −I ions. These geometries were then optimized using the DFT method (see computational details; see Tables S37−S48 and Figures S33−S45).

Among all the models tested, Dy(III) with axial −F was found to diminish the ground state QTM significantly, thus presumably offering a viable synthetic strategy to isolate a zero-field SMM. However, the out-of-plane distortion ($\tau$) of Dy(III) in the Dy−F model is found to be 0.64 Å which is lower than that found for THF, but as stated earlier, a combination of a strong axial crystal field coupled with a large $\tau$ value is important to quench the ground state QTM and increase the energy gap between the ground state KD and the other excited state KDs'. Although −F substitution offers a strong axiality (see LoProp charges and crystal field parameters in the Supporting Information), the $\tau$-value is smaller than the THF ligand. Therefore, in the Dy−F model, we have a counterbalancing act. This finding will be extremely helpful for the synthetic chemist to engineer the Ln(III) magnetic properties (Figure 8). For Yb(III), on the other hand, the

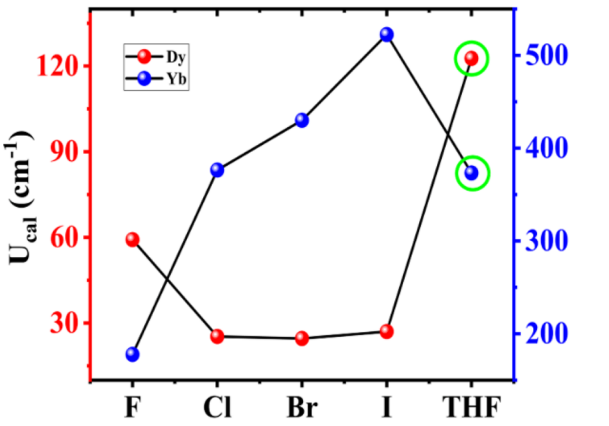


**Figure 8.** Comparison of the calculated effective energy barrier with different axial ligands. The green circles indicate the parent complexes **1** and **2**.

Yb(III)−I model was found to offer a great advantage as the Yb−I distance was found to be 2.99 Å, leading to weakening of the axial ligand and to relaxation via the fourth excited state KD, enhancing the computed barrier height significantly (see Figures 8 and 9).

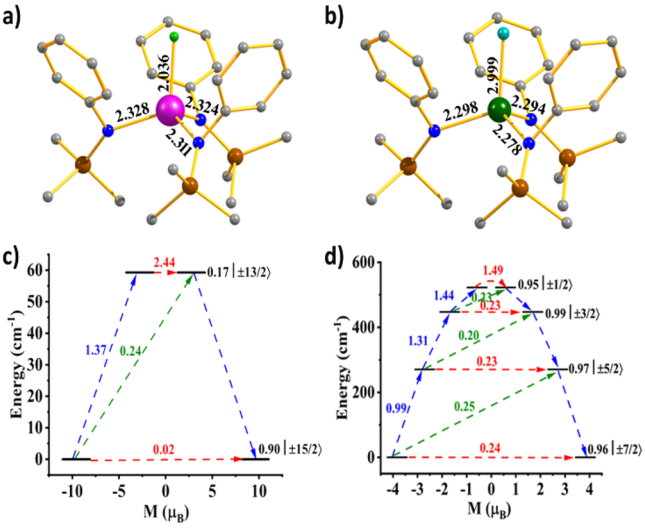


**Figure 9.** (a, b) The optimized geometry along with the bond lengths with the first coordination atoms. (c, d) The plausible relaxation mechanisms of Dy−F and Yb−I, respectively.

## CONCLUSION

In this report, we have unveiled a series of low coordinate Ln(III) molecular complexes with the general molecular formula of [Ln(N-TMSA)$_3$(THF)], where Ln = Dy (**1**) or Yb (**2**), which are structurally characterized. The packing diagram and Hirshfeld surface analysis undeniably disclose that the intermolecular interactions are extremely weak or nil. The dc susceptibility measurements performed on these complexes illustrate the presence of magnetic anisotropy associated with **1** and **2**, as expected for the anisotropic Dy(III) and Yb(III) ions. The ac relaxation dynamic studies reveal that $\chi_M''$ signals were observed only in the presence of an optimum external field with a barrier height of 46 and 40 K, respectively, for **1** and **2**. The detailed electronic structure and the mechanism of magnetization relaxation were investigated using *ab initio*


https://doi.org/10.1021/acs.cgd.2c01246
Cryst. Growth Des. 2023, 23, 629−636

methods. Further, the calculation unveils that the crystal field around the lanthanides is better suited for a prolate ion than the oblate ion. Therefore, the removal of the coordinated THF molecule in **2** and other related prolate lanthanide complexes (such as Er(III)) in its three-coordinate planar geometry is targeted in our laboratory. Overall, we have shed light on the influence of distorted tetrahedral coordination geometry on the electronic structure and magnetization relaxation dynamics of Ln(III) complexes, through the combined experimental and theoretical investigations, which is extremely rare in the literature.

## ■ ASSOCIATED CONTENT

### Supporting Information

The Supporting Information is available free of charge at https://pubs.acs.org/doi/10.1021/acs.cgd.2c01246.

Materials and methods, computational details, crystallographic parameters, supporting magnetic data, and energetics of KD (PDF)

### Accession Codes

CCDC 2216479−2216480 contain the supplementary crystallographic data for this paper. These data can be obtained free of charge via www.ccdc.cam.ac.uk/data_request/cif, or by emailing data_request@ccdc.cam.ac.uk, or by contacting The Cambridge Crystallographic Data Centre, 12 Union Road, Cambridge CB2 1EZ, UK; fax: +44 1223 336033.

## ■ AUTHOR INFORMATION


### Corresponding Authors

**Maheswaran Shanmugam** − *Department of Chemistry, Indian Institute of Technology Bombay, Mumbai, Maharashtra 400076, India;* orcid.org/0000-0002-9012-743X; Email: eswar@chem.iitb.ac.in

**Gopalan Rajaraman** − *Department of Chemistry, Indian Institute of Technology Bombay, Mumbai, Maharashtra 400076, India;* orcid.org/0000-0001-6133-3026; Email: rajaraman@chem.iitb.ac.in

### Authors

**Dipanti Borah** − *Department of Chemistry, Indian Institute of Technology Bombay, Mumbai, Maharashtra 400076, India*

**Amaleswari Rasamsetty** − *Department of Chemistry, Indian Institute of Technology Bombay, Mumbai, Maharashtra 400076, India*

**Deepanshu Chauhan** − *Department of Chemistry, Indian Institute of Technology Bombay, Mumbai, Maharashtra 400076, India*

**Shalini Tripathi** − *Department of Chemistry, Indian Institute of Technology Bombay, Mumbai, Maharashtra 400076, India*

**Felix Houard** − *Univ Rennes, INSA Rennes, CNRS, ISCR (Institut des Sciences Chimiques de Rennes), UMR 6226, F 35000 Rennes, France;* orcid.org/0000-0003-3991-8954

**Olivier Cador** − *Univ Rennes, INSA Rennes, CNRS, ISCR (Institut des Sciences Chimiques de Rennes), UMR 6226, F 35000 Rennes, France;* orcid.org/0000-0003-2064-6223

**Kevin Bernot** − *Univ Rennes, INSA Rennes, CNRS, ISCR (Institut des Sciences Chimiques de Rennes), UMR 6226, F 35000 Rennes, France; Institut Universitaire de France, 75005 Paris, France;* orcid.org/0000-0001-8337-6246

Complete contact information is available at: https://pubs.acs.org/10.1021/acs.cgd.2c01246

### Author Contributions

‖D.B. and A.R. contributed equally.


### Notes

The authors declare no competing financial interest.

## ■ ACKNOWLEDGMENTS

M.S. wishes to thank the funding agencies SERB (CRG/2019/004185 and SPR/2019/001145), CSIR (09/087(1060)/2020-EMR-I), and IIT Bombay for financial support. D.B. thanks CSIR for the fellowship. G.R. would like to acknowledge SERB (CRG/2018/00430, SB/SJF/2019-20/12) and SPR/2019/001145. K.B. thanks Institut des Sciences Chimiques de Rennes, France for providing the SQUID Magnetometer facility.

## ■ ABBREVIATIONS

N-TMSA, Trimethylsilylanilide; THF, Tetrahydrofuran; CShM, Continuous Shape Measurement; HS, Hirshfeld Surface; DC, Direct Current; AC, Alternating Current; QTM, Quantum Tunneling of Magnetization; CASSCF, Complete Active Space Self-Consistent Field; RASSI, Restricted Active Space State Interaction; KD, Kramers Doublet

## ■ REFERENCES


(1) Blagg, R. J.; Ungur, L.; Tuna, F.; Speak, J.; Comar, P.; Collison, D.; Wernsdorfer, W.; McInnes, E. J. L.; Chibotaru, L. F.; Winpenny, R. E. P. Magnetic relaxation pathways in lanthanide single-molecule magnets. *Nat. Chem.* **2013**, *5* (8), 673−678.

(2) Liu, J.; Chen, Y.-C.; Liu, J.-L.; Vieru, V.; Ungur, L.; Jia, J.-H.; Chibotaru, L. F.; Lan, Y.; Wernsdorfer, W.; Gao, S.; Chen, X.-M.; Tong, M.-L. A Stable Pentagonal Bipyramidal Dy(III) Single-Ion Magnet with a Record Magnetization Reversal Barrier over 1000 K. *J. Am. Chem. Soc.* **2016**, *138* (16), 5441−5450.

(3) Woodruff, D. N.; Winpenny, R. E. P.; Layfield, R. A. Lanthanide Single-Molecule Magnets. *Chem. Rev.* **2013**, *113* (7), 5110−5148.

(4) Ishikawa, N.; Sugita, M.; Ishikawa, T.; Koshihara, S.-y.; Kaizu, Y. Lanthanide Double-Decker Complexes Functioning as Magnets at the Single-Molecular Level. *J. Am. Chem. Soc.* **2003**, *125* (29), 8694−8695.

(5) Mannini, M.; Pineider, F.; Sainctavit, P.; Danieli, C.; Otero, E.; Sciancalepore, C.; Talarico, A. M.; Arrio, M.-A.; Cornia, A.; Gatteschi, D.; Sessoli, R. Magnetic memory of a single-molecule quantum magnet wired to a gold surface. *Nat. Mater.* **2009**, *8* (3), 194−197.

(6) Bogani, L.; Wernsdorfer, W. Molecular spintronics using single-molecule magnets. *Nat. Mater.* **2008**, *7* (3), 179−186.

(7) Leuenberger, M. N.; Loss, D. Quantum computing in molecular magnets. *Nature* **2001**, *410* (6830), 789−793.

(8) Wernsdorfer, W.; Sessoli, R. Quantum Phase Interference and Parity Effects in Magnetic Molecular Clusters. *Science* **1999**, *284* (5411), 133−135.

(9) Winpenny, R. E. P. Quantum Information Processing Using Molecular Nanomagnets As Qubits. *Angew. Chem., Int. Ed.* **2008**, *47* (42), 7992−7994.

(10) Chilton, N. F.; Collison, D.; McInnes, E. J. L.; Winpenny, R. E. P.; Soncini, A. An electrostatic model for the determination of magnetic anisotropy in dysprosium complexes. *Nat. Commun.* **2013**, *4* (1), 2551.

(11) Rinehart, J. D.; Long, J. R. Exploiting single-ion anisotropy in the design of f-element single-molecule magnets. *Chem. Sci.* **2011**, *2* (11), 2078−2085.

(12) Ungur, L.; Chibotaru, L. F. Strategies toward High-Temperature Lanthanide-Based Single-Molecule Magnets. *Inorg. Chem.* **2016**, *55* (20), 10043−10056.

(13) Dey, A.; Kalita, P.; Chandrasekhar, V. Lanthanide(III)-Based Single-Ion Magnets. *ACS Omega* **2018**, *3* (8), 9462−9475.

(14) Canaj, A. B.; Singh, M. K.; Regincós Marti, E.; Damjanović, M.; Wilson, C.; Céspedes, O.; Wernsdorfer, W.; Rajaraman, G.; Murrie, M. Boosting axiality in stable high-coordinate Dy(iii) single-molecule magnets. *Chem. Commun.* **2019**, *55* (42), 5950−5953.
(15) Singh, S. K.; Gupta, T.; Rajaraman, G. Magnetic Anisotropy and Mechanism of Magnetic Relaxation in Er(III) Single-Ion Magnets. *Inorg. Chem.* **2014**, *53* (20), 10835−10845.
(16) Goodwin, C. A. P.; Ortu, F.; Reta, D.; Chilton, N. F.; Mills, D. P. Molecular magnetic hysteresis at 60 K in dysprosocenium. *Nature* **2017**, *548* (7668), 439−442.
(17) Guo, F.-S.; Day, B. M.; Chen, Y.-C.; Tong, M.-L.; Mansikkamäki, A.; Layfield, R. A. Magnetic hysteresis up to 80 K in a dysprosium metallocene single-molecule magnet. *Science* **2018**, *362* (6421), 1400−1403.
(18) Vanjak, J. C.; Wilkins, B. O.; Vieru, V.; Bhuvanesh, N. S.; Reibenspies, J. H.; Martin, C. D.; Chibotaru, L. F.; Nippe, M. A High-Performance Single-Molecule Magnet Utilizing Dianionic Aminoborolide Ligands. *J. Am. Chem. Soc.* **2022**, *144* (39), 17743−17747.
(19) Gupta, S. K.; Rajeshkumar, T.; Rajaraman, G.; Murugavel, R. An unprecedented zero field neodymium(iii) single-ion magnet based on a phosphonic diamide. *Chem. Commun.* **2016**, *52* (44), 7168−7171.
(20) Chen, Y.-C.; Liu, J.-L.; Ungur, L.; Liu, J.; Li, Q.-W.; Wang, L.-F.; Ni, Z.-P.; Chibotaru, L. F.; Chen, X.-M.; Tong, M.-L. Symmetry-Supported Magnetic Blocking at 20 K in Pentagonal Bipyramidal Dy(III) Single-Ion Magnets. *J. Am. Chem. Soc.* **2016**, *138* (8), 2829−2837.
(21) Liu, J.-L.; Chen, Y.-C.; Zheng, Y.-Z.; Lin, W.-Q.; Ungur, L.; Wernsdorfer, W.; Chibotaru, L. F.; Tong, M.-L. Switching the anisotropy barrier of a single-ion magnet by symmetry change from quasi-D5h to quasi-Oh. *Chem. Sci.* **2013**, *4* (8), 3310−3316.
(22) Li, J.; Gómez-Coca, S.; Dolinar, B. S.; Yang, L.; Yu, F.; Kong, M.; Zhang, Y.-Q.; Song, Y.; Dunbar, K. R. Hexagonal Bipyramidal Dy(III) Complexes as a Structural Archetype for Single-Molecule Magnets. *Inorg. Chem.* **2019**, *58* (4), 2610−2617.
(23) Li, Z.-H.; Zhai, Y.-Q.; Chen, W.-P.; Ding, Y.-S.; Zheng, Y.-Z. Air-Stable Hexagonal Bipyramidal Dysprosium(III) Single-Ion Magnets with Nearly Perfect D6h Local Symmetry. *Chem.—Eur. J.* **2019**, *25* (71), 16219−16224.
(24) Ding, Y.-S.; Blackmore, W. J. A.; Zhai, Y.-Q.; Giansiracusa, M. J.; Reta, D.; Vitorica-Yrezabal, I.; Winpenny, R. E. P.; Chilton, N. F.; Zheng, Y.-Z. Studies of the Temperature Dependence of the Structure and Magnetism of a Hexagonal-Bipyramidal Dysprosium(III) Single-Molecule Magnet. *Inorg. Chem.* **2022**, *61* (1), 227−235.
(25) Canaj, A. B.; Dey, S.; Wilson, C.; Céspedes, O.; Rajaraman, G.; Murrie, M. Engineering macrocyclic high performance pentagonal bipyramidal Dy(iii) single-ion magnets. *Chem. Commun.* **2020**, *56* (80), 12037−12040.
(26) Langley, S. K.; Vignesh, K. R.; Holton, K.; Benjamin, S.; Hix, G. B.; Phonsri, W.; Moubaraki, B.; Murray, K. S.; Rajaraman, G. Mononuclear Dysprosium(III) Complexes with Triphenylphosphine Oxide Ligands: Controlling the Coordination Environment and Magnetic Anisotropy. *Inorganics* **2018**, *6*, 61.
(27) Bar, A. K.; Kalita, P.; Singh, M. K.; Rajaraman, G.; Chandrasekhar, V. Low-coordinate mononuclear lanthanide complexes as molecular nanomagnets. *Coord. Chem. Rev.* **2018**, *367*, 163−216.
(28) Rasamsetty, A.; Mehta, S.; Ansari, K. U.; Kumar, P.; Mondal, A.; Shanmugam, M. Six-coordinated dinuclear lanthanide(iii) amide complexes: investigation of magnetization relaxation dynamics and their electronic structures. *Dalton Transactions* **2021**, *51* (1), 63−68.
(29) Das, C.; Upadhyay, A.; Shanmugam, M. Influence of Radicals on Magnetization Relaxation Dynamics of Pseudo-Octahedral Lanthanide Iminopyridyl Complexes. *Inorg. Chem.* **2018**, *57* (15), 9002−9011.
(30) Parmar, V. S.; Mills, D. P.; Winpenny, R. E. P. Mononuclear Dysprosium Alkoxide and Aryloxide Single-Molecule Magnets. *Chem.—Eur. J.* **2021**, *27* (28), 7625−7645.
(31) Yu, K.-X.; Ding, Y.-S.; Han, T.; Leng, J.-D.; Zheng, Y.-Z. Magnetic relaxations in four-coordinate Dy(iii) complexes: effects of anionic surroundings and short Dy−O bonds. *Inorg. Chem. Front.* **2016**, *3* (8), 1028−1034.
(32) Parmar, V. S.; Gransbury, G. K.; Whitehead, G. F. S.; Mills, D. P.; Winpenny, R. E. P. Slow magnetic relaxation in distorted tetrahedral Dy(iii) aryloxide complexes. *Chem. Commun.* **2021**, *57* (73), 9208−9211.
(33) Brown, A. J.; Pinkowicz, D.; Saber, M. R.; Dunbar, K. R. A Trigonal-Pyramidal Erbium(III) Single-Molecule Magnet. *Angewandte Chemie (International ed. in English)* **2015**, *54* (20), 5864−5868.
(34) Zhang, P.; Jung, J.; Zhang, L.; Tang, J.; Le Guennic, B. Elucidating the Magnetic Anisotropy and Relaxation Dynamics of Low-Coordinate Lanthanide Compounds. *Inorg. Chem.* **2016**, *55* (4), 1905−1911.
(35) Harriman, K. L. M.; Murillo, J.; Suturina, E. A.; Fortier, S.; Murugesu, M. Relaxation dynamics in see-saw shaped Dy(iii) single-molecule magnets. *Inorg. Chem. Front.* **2020**, *7* (24), 4805−4812.
(36) Moehring, S. A.; Ziller, J. W.; Evans, W. J. Rare-earth complexes of the asymmetric amide ligands, N(SiMe3)Ph and N(SiMe3)Cy. *Polyhedron* **2019**, *168*, 72−79.
(37) Pinsky, M.; Avnir, D. Continuous Symmetry Measures. 5. The Classical Polyhedra. *Inorg. Chem.* **1998**, *37* (21), 5575−5582.
(38) Seitz, M.; Oliver, A. G.; Raymond, K. N. The Lanthanide Contraction Revisited. *J. Am. Chem. Soc.* **2007**, *129* (36), 11153−11160.
(39) Rudowicz, C.; Chua, M.; Reid, M. F. On the standardization of crystal-field parameters and the multiple correlated fitting technique: Applications to rare-earth compounds. *Physica B: Condensed Matter* **2000**, *291* (3), 327−338.
(40) Gagliardi, L.; Lindh, R.; Karlström, G. Local properties of quantum chemical systems: The LoProp approach. *J. Chem. Phys.* **2004**, *121* (10), 4494−4500.
(41) Singh, S. K.; Gupta, T.; Shanmugam, M.; Rajaraman, G. Unprecedented magnetic relaxation via the fourth excited state in low-coordinate lanthanide single-ion magnets: a theoretical perspective. *Chem. Commun.* **2014**, *50* (98), 15513−15516.


https://doi.org/10.1021/acs.cgd.2c01246
*Cryst. Growth Des.* 2023, 23, 629−636